

Terahertz performance of quasioptical front-ends with a hotelectron bolometer

This article has been downloaded from IOPscience. Please scroll down to see the full text article.

2006 J. Phys.: Conf. Ser. 43 1294

(<http://iopscience.iop.org/1742-6596/43/1/316>)

View [the table of contents for this issue](#), or go to the [journal homepage](#) for more

Download details:

IP Address: 38.107.179.211

The article was downloaded on 16/02/2012 at 02:41

Please note that [terms and conditions apply](#).

Terahertz performance of quasioptical front-ends with a hot-electron bolometer

A Semenov¹, H Richter¹, B Günther¹, H-W Hübers¹ and J Karamarkovic²

¹DLR Institute of Planetary Research, Rutherfordstrasse 2, 12489 Berlin, Germany

²University of Nis, Aleksandra Medvedeva 14, 18000 Nis, Serbia and Montenegro

alexei.semenov@dlr.de

Abstract. We present terahertz performance of quasioptical front-ends consisting of a hot-electron bolometer imbedded in a planar feed antenna and integrated with an immersion lens. The impedance and radiation pattern of the log-spiral and double-slot planar feeds are evaluated using the method of moments; the collimating action of the lens is modelled using the physical optics. The total efficiency of the front-ends is computed taking into account frequency dependent impedance of the bolometer. Measured performance of the front-ends qualifies the simulation technique as a reliable tool for the design of terahertz receivers.

1. Introduction

Exploring the terahertz frequency range becomes an important trend in planetary science, astronomy and security research. For terahertz receivers the planar integrated quasioptical technology is expected to be a preferable alternative to wave-guide based front ends. Recent progress in nano-structuring and micro machining allows reliably producing and aligning planar antenna structures on dielectric surfaces with an accuracy sufficient for terahertz range. Versatile feed antennas integrated with immersion lenses have been shown to couple radiation to superconducting detectors. However, designing an integrated quasioptical front-end requires reliable modelling of the feed-antenna performance in combination with the particular detector. A semi-analytical, lumped element technique provides results inconsistent with the experimental data at frequencies above a few terahertz [1]. The main reason, e.g. for a double-slot feed, is that this technique neglects frequency-dependent detector impedance and also parasitic impedances appearing at the points where virtual lumped elements are connected to each other.

In this work we apply the method of moments (MoM) to the entire feed structure including imbedding and interconnecting elements. The MoM solution is then used as an input for the physical-optics ray-tracing procedure in order to obtain the beam parameters of the integrated lens antenna. We compute an efficiency of the front-ends taking into account the impedance of the bolometer coupled to the feed. We further compare simulated and measured performance of integrated planar double-slot and log-spiral antennas to verify this technique at frequencies from 1.5 THz to 5 THz.

2. Simulation procedure

The full wave method of moments reveals the current and charge distribution in the antenna by solving numerically Maxwell equations with boundary conditions on a virtual mesh superimposed on the real

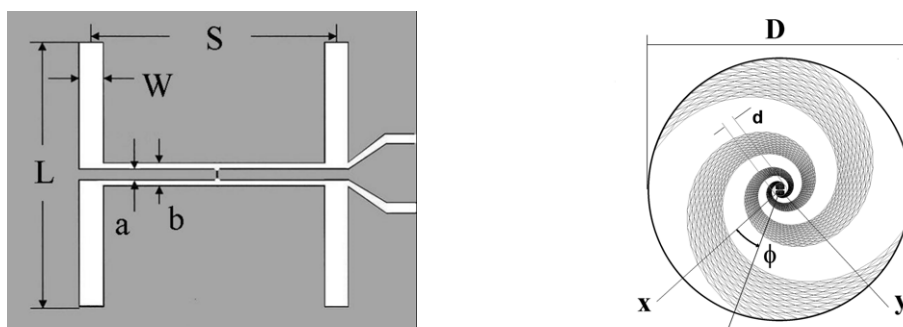


Fig.1 Layout of a double-slot (left) and a log-spiral (right) feeds. Grey colour shows the gold layer. The mesh and the coordinate system used for FEKO simulations are shown for the log-spiral feed .

structure. The fields in an observation point can be computed via scalar and vector potentials generated by the currents. We used FEKO software (<http://www.feko.info/>) that utilizes this technique.

The layout of studied double-slot and logarithmic spiral feeds are defined in Fig. 1 and Table 1. The rectangle in the geometric centre of each feed depicts a detector, which is used for experimental characterization of the integrated antenna. MoM simulations were made for feeds printed from a 70-nm thick gold layer on Si half-space. The double-slot feeds (left panel) were cut from a $100 \times 100 \mu\text{m}^2$ rectangle. For a log-spiral feed (right panel) the outer diameter (D) is the diameter of the circle that encompasses the feed structure. The inner diameter (d) is the smallest diameter where the arms still obey the spiral equation. The parameter $\alpha = 0.36$ [2] was chosen to build the feed according to $R = R_0 \exp(\alpha\phi)$ with ϕ been the angle and R the distance from the geometric center of the feed. We used a uniform voltage excitation along the infinitesimally thin slit located at the detector site.

Simulated impedance for the TWS2 and DLR_c feeds are shown in Fig. 2. For the TWS2 feed, the frequency dependence of the real and imaginary parts of the feed impedance seen from the excitation slit has a certain similarity to the frequency dependence of the impedance computed for two slots without connecting co-planar waveguide [3]. However, changes introduced by the co-planar waveguide are clearly visible. The radiation coupling efficiency of the feed antenna reaches the maximum value when the imaginary component of the impedance becomes zero. For our TWS2 feed corresponding resonance frequency appears between 2.2 and 2.5 THz. In the receiving mode, the frequency resulting in the best coupling also depends on the impedance of the detector connected to the feed. The impedance of the DLR_c feed has a non-negligible imaginary component in the whole frequency range of simulation. That contradicts to the Babinet principle suggesting a real impedance for a complementary planar antenna. The real part of the impedance remains almost constant and exceeds noticeably the imaginary component only at frequencies below 2.5 THz. Thus our DLR_c feed may be qualified as frequency-independent in the frequency interval from 1 THz to 2.5 THz.

For all studied feeds MoM simulations provide the Rayleigh distance less than one millimetre that is far less than the diameter of our immersion lens. Therefore, as an input for the ray-tracing procedure we used the far-field results delivered by the MoM. The electric and magnetic fields at the surface inside the lens was decomposed into the s- and p-components. Then each component was multiplied with an appropriate Fresnel transmission coefficient and resulting components were combined

Table 1. Sizes of the studied double-slot and log-spiral feeds.

| Feed | a, μm | b, μm | L, μm | S, μm | W, μm | D, μm | d, μm | α , rad^{-1} |
|-------|------------------|------------------|------------------|------------------|------------------|------------------|------------------|------------------------------|
| TWS1 | 2 | 4 | 60 | 32 | 4 | -- | -- | -- |
| TWS2 | 2.2 | 3.3 | 40 | 21 | 2.2 | -- | -- | -- |
| TWS6 | 2 | 4 | 50 | 28 | 3.6 | -- | -- | -- |
| DLR_a | -- | -- | -- | -- | -- | 130 | 11.2 | 0.36 |
| DLR_c | -- | -- | -- | -- | -- | 48 | 2.25 | 0.36 |

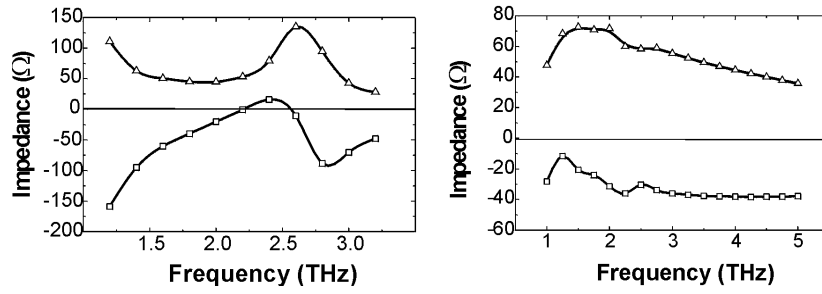


Fig. 2 Real (triangles) and imaginary (squares) components of the impedance computed with MoM for the TWS2 (left) and the DLR_c (right) feeds. Lines are guides for the eyes.

again to obtain the electric E and magnetic H fields just outside the lens. Equivalent electric and magnetic sources outside the lens were defined [4] as

$$\vec{J}_s = \vec{n}1 \times \vec{H} \quad \text{and} \quad \vec{M}_s = -\vec{n}1 \times \vec{E} \tag{1}$$

where $\vec{n}1$ is the unit vector normal to the lens surface. Electric field at a distance r from the running point on the surface, \vec{e}_r been the unit vector, was obtained integrating over the lens surface A

$$\vec{E} = \frac{jk_0}{4\pi\omega\epsilon_0} \times \iint_S \left[\vec{J}_s - (\vec{J}_s \cdot \vec{e}_r)\vec{e}_r + \frac{1}{Z_0} (\vec{M}_s \times \vec{e}_r) \right] \frac{e^{-jk_0r}}{r} dA \tag{2}$$

with k_0 , Z_0 and ω been the free-space wave-vector, the impedance of free space and the angular frequency, respectively. We computed the beam profile for the extended hemi-spherical lens (radius $R_L = 6$ mm, refraction index $n = 3.42$) varying the extension lengths ϵ . For the TWS6 feed an acceptable level (-14 dB) of side lobes are both achieved at $\epsilon = 2.45$ mm that brings the feed almost to the focal point $\epsilon = R_L/(n-1)$ of a corresponding elliptical lens [5]. The beam profile was almost the same in both E- and H-planes down to -15 dB. For the log-spiral feed we found the same optimal extension that resulted, however, in a not symmetric beam and side-lobes varying with ϕ .

3. Experimental arrangement

We studied experimentally the performance of integrated lens antennas in the receiving mode. A hot-electron bolometer (HEB) was incorporated in the feed. The feeds were printed on a 350 μm thick Si substrate from a 70 nm thick gold film. HEBs were produced from NbN films with a nominal thickness of about 5 nm. The typical normal-state resistance $R_n = 100 \pm 15 \Omega$ was larger than the

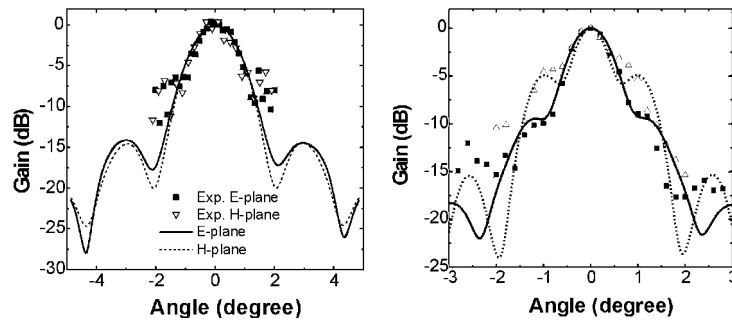


Fig. 3 Simulated (lines) and measured (symbols) beam pattern of the front-ends with the TWS6 feed at 1.9 THz (left) and the DLR_a feed at 2.5 THz (right) for $\phi = 35^\circ$ (triangle) and 135° (squares).

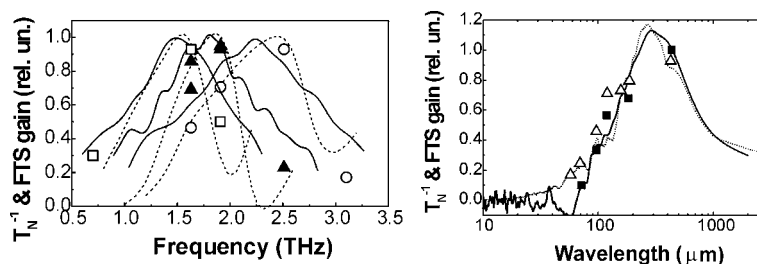


Fig. 4 Simulated gain (dotted lines), FTS spectra (solid lines) and reciprocal noise temperature of integrated antennas with TWS1 (squares), TWS6 (triangles) and TWS2 (circles) feeds.

accuracy of the manufacturing process and the film sheet resistance suggested. An excess resistance due to contacts between the bolometer and the feed varied from 30% to 50% of the R_n . The substrate with the feed and the bolometer was glued onto the flat cut of an extended 12-mm hemispherical silicon lens. The total extension amounted at 2.45 mm. In the heterodyne regime, a THz gas laser providing lines at frequencies 0.69, 1.63, 2.53, and 3.1 THz was used as a local oscillator. The double sideband noise temperature was measured by the Y-factor method. The beam pattern of the integrated antenna was obtained with a 5 mm mercury lamp moving in the far field of the integrated antenna. Fast-Fourier-Transform (FTS) measurements were performed with the HEB kept in the middle of the superconducting transition and operated in the direct detection regime.

4. Experimental data versus simulations

The measured beam pattern of the integrated lens antennas with the TWS6 feed and DLR_C feed at are shown in Fig. 3 along with the computed beam profiles. Due to the large distance between the lamp and the antenna, the nose level was relatively high not allowing us to clearly distinguish side-lobes. However, an overall width of the main lobe corresponds fairly well with the results of simulation. In order to evaluate the gain of the antenna, we assumed a frequency independent conversion efficiency of the HEB and took into account the skin effect in the bolometer itself [5]. This yields a complex impedance of the bolometer Z_B resulting in the following antenna gain G

$$Z_B = R_n \frac{w(1+j)}{4\delta} \coth \left[\frac{w(1+j)}{4\delta} \right] = Z_{B1} + jZ_{B2}; \quad G = \frac{4Z_{B1}(Z_1 + Z_K) + Z_{B2}Z_2}{(Z_1 + Z_{B1} + Z_K)^2 + (Z_2 + Z_{B2})^2} M \quad (3)$$

where $Z_A = Z_1 + jZ_2$ is the impedance of the feed, Z_K is the contact resistance and $\delta = (2\mu_0\omega/\rho)^{1/2}$ and ρ are the skin depth and the normal-state resistivity of the bolometer, respectively. The factor M accounts for coupling losses, which have been estimated using attenuation of optical elements. For gain simulations we used $Z_K = 0.4 R_n$. For all studied feeds we have found a reasonably good agreement between measured FTS spectrum, system noise temperatures and simulated (Eq. 3) antenna gain. Data for selected feeds are presented in Fig. 4. Measured noise temperatures correlate better with simulated gain spectra than with FTS spectra, which are systematically shifted to lower frequencies.

In conclusion, we have demonstrated that the full method of moments applied to the entire feed structure and combined with the physical-optics ray-tracing adequately models both the radiation coupling and the beam pattern of terahertz quasioptical front-ends with hot-electron bolometers.

References

- [1] R.A. Wyss et al., in Proceedings of the 11th Int. Symposium on Space Terahertz Technology, Uni. of Michigan, Ann Arbor, MI, pp. 388-397, May 2000.
- [2] Yu.P. Gousev et al., Appl. Phys. Lett. **69**(5), 691-693 (1996).
- [3] M. Kominami et al., IEEE Transactions on Antennas and Propagations **33**, 600 (1985).
- [4] J.A. Balanis, Antenna Theory: Analysis and Design, John Wiley & Sons, Inc., p. 448, 1982.
- [5] A.D. Semenov et al., Journal of Applied Physics **88**, 6758 (2000).